# Study on Europium Doped Hydroxyapatite Nanoparticles by Fourier Transform Infrared Spectroscopy and Their Antimicrobial Properties

Simona Liliana Iconaru, Mikael Motelica-Heino, Daniel Predoi

# Study on europium doped hydroxyapatite nanoparticles by Fourier transform infrared spectroscopy and their antimicrobial properties

Simona Liliana Iconaru[1,2], Mikael Motelica-Heino[2], Daniela Predoi[1*]

[1]Department of Multifunctional Materials and Structures Laboratory, National Institute of Materials Physics, 105 BisAtomistilor, P.O. Box MG 07, 077125 Magurele, Romania,[1*]dpredoi@gmail.com

[2]ISTO, Université d'Orléans, Orléans cedex 02, 45067, France

## Abstract

In this work, Fourier Transform Infrared spectroscopy (FT-IR) analysis were conducted on europium doped hydroxyapatite, $Ca_{10-x}Eu_x(PO_4)_6(OH)_2$ nanocrystalline powders (Eu:HAp) with $0 \leq x_{Eu} \leq 0.2$. Antimicrobial studies were also performed for the first time on Eu:Hap. The antimicrobial properties of Eu:HAp nanoparticles with $0 \leq x_{Eu} \leq 0.2$ on Gram-negative (*E coli ATCC 25922*, *Pseudomonas aeruginosa 1397) and Gram-positive (Staphylococcus aureus 0364*, *Enterococcus faecalis ATCC 29212*) bacteria systems and a species of fungus (*Candida albicans ATCC 10231*) were reported. Our study demonstrates that the antimicrobial activity of Eu:HAp nanoparticles is dependent on the europium concentration.

**Keywords**: nanocrystalline, hydroxyapatite, europium, antimicrobial activity.

## 1. Introduction

Hydroxyapatite ( $Ca_{10}(PO_4)_6(OH)_2$ ) is the main inorganic component of human bones and teeth, showing a very good biocompatibility, bioactivity and osteoconductivity due to its nontoxic, and noninflammatory properties [1-9]. Therefore, it has been widely used in many fields, like bio-medical applications, as a bioactive coating material for metallic implants, clinical bone augmentation, dental implantology, tumors treatment and cell activation, or it could be also used as a carrier in drug delivery systems [10]. Moreover, trivalent rare-earth-

ion-doped hydroxyapatite can also be used as biological fluorescent probes due to their excelent luminescent properties.

In the last years, luminescence imagining, especially in the region of near-infrared spectrum showed a great interest for biomedical applications, focusing on the development and characterization of rare-earth based inorganic luminescent nanoparticules [11-14]. The most important applications could be found on pharmaceutical industry or biological and medical diagnostics [15-17].

When doped with rare-earth ions, hydroxyapatite is being considered a fluorescent probe, the luminescence intensity depending on the concentration of rare-earth's doping ions, the degree of crystallinity and the crystal structure of the host material [18-20]. Over the past decade, several methods for obtaining luminescent inorganic nanoparticles have been developed, including coprecipitation and sol-gel synthesis which allow to adjust particles morphology, size, structure and composition in order to adapt their physical and chemical properties [14, 21-23].

Fluorescent labeling is an indispensable technique which is widely used for performing nondestructive observations both in vivo and in vitro by replacing the calcium ions in hydroxyapatite crystal lattice using rare earth luminescent ions [24-26]. The hexagonal hydroxyapatite allows the substitutions of many rare earth ions without any changes in the crystal structure [27-30]. Nowadays, the rare earths ions doped hydroxyapatite nanoparticles are being studied very intently as cell labeling materials, as a result of their strong luminescence under visible light spectrum. [31-36]

Compared to other rare earth elements, trivalent Europium $Eu^{3+}$ ions have a simple electronic energy level scheme and hypersensitive transitions. The $Eu^{3+}$ doped calcium apatites represent a good biological probe candidate due to their low toxicity and stable luminescence over time and it has been proven that a small amount of europium in the bioactivity behaviour has no harmful effects [37-41]. The ionic radius similarity between $Ca^{2+}$ and $Eu^{3+}$ in the apatite lattice makes them a good host for $Eu^{3+}$ doping [4].

Recently, great attention has been paid to europium doped hydroxyapatite (Eu:HAp) potential use as biological probe [30]. Previously, the europium doped hydroxyapatite was studied applying PL [32-33]. On the other hand, IR spectroscopy is a powerful method in ionic investigation and has been used extensively in phosphate minerals research [42–44].

Concerning the phase composition of the as-prepared Eu:HAp various studies have been reported [31-33, 45]. In our recent studies no other additional phases were observed [45] for the synthesized Eu:HAp samples and the diffraction patterns were identical to that

obtained for stoichiometric apatite. In this paper, the obtained Eu:Hap samples were systematically characterized by Fourier transform infrared (FTIR) spectroscopy. The aim of this work is to contribute to the study of the influence of europium in the structure of hydroxyapatite. On the other hand, cell viability from various doses of the Eu:HAp samples at two different time points were compared with corresponding culture media values.After 24 h and 48h exposure to all types of Eu:HAp at 10 μg /ml concentration, the morphology of the cells was preserved. Moreover, we report in this work for the first time the bacterial studies on Eu:HAp. Furthermore, in this article, original stidies on antimicrobial activities of Eu:HAp against Gram-positive (*Staphylococcus aureus 0364, Enterococcus faecalis ATCC 29212*), Gram-negative (*E coli* ATCC 25922, *Pseudomonas aeruginosa* 1397) and fungal strains (*Candida albicans* ATCC 10231) are presented.

## 2. Materials and methods

### 2.1. Samples

All the reagents for synthesis, including ammonium dihydrogen phosphate [$(NH_4)_2HPO_4$], calcium nitrate [Ca $(NO_3)_2 \cdot 4H_2O$], and europium nitrate [$Eu(NO_3)_3 \cdot 6H_2O$] (Alpha Aesare) were used as purchased, without purification. Europium doped hydroxyapatite (Eu:Hap, $Ca_{10-x}Eu_x(PO_4)_6(OH)_2$) nanoparticles were performed by setting $x_{Eu}$ = 0.01, $x_{Eu}$ = 0.02,$x_{Eu}$ = 0.05, $x_{Eu}$ = 0.1, $x_{Eu}$ = 0.2 and [Ca+Eu]/P as 1.67 in accord with [45].

### 2.2. Fouriertransforms infrared (FTIR) spectroscopy.

The functional groups present in the prepared nanoparticles and thin films were identified by FTIR using a Perkin Elmer, Spectrum BX spectrometer. In order to obtain the nanoparticles spectra, 1% of the nanopowder was mixed and ground with 99% KBr. Tablets of 10 mm diameter were prepared by pressing the powder mixture with a pressure of not more than 10 psi. The spectrum was recorded in the range of 400 to 4000 $cm^{-1}$ with 4 $cm^{-1}$ resolution. The first FTIR spectra were obtained after 256 scans at room temperature(25 ± $0.5^0$C). The second derivative IR spectra were acquired after 5-point smoothing of the original IR spectra.For selected spectral ranges, the peak fitting analyses were performed using procedures of J. Kolmas et al. [46]: (i) baseline correction, (ii) second derivative

calculation and self deconvolution assessment in order to determine the number and positions of the bands and (iii) curve fittings with fixed peak positions using Lorentzienne lines. In the previous studies Matsuhiro et al. [47] and Gómez-Ordóñezet al. [48] showed thatsecond-derivatives of FTIR spectra are generally used as an aid for wave number determination of weak absorption bands onto improve resolution of overlapped bands in the originalspectra.To that end, in our studies derivation including Savitzky-Golay algorithm with nine smoothing points was performed.

### 2.3. Antimicrobial studies.

The microbial strains identification was confirmed by aid of VITEK II automatic system. VITEK cards for identification and susceptibility testing were inoculated and incubated according to the manufacturer's recommendations. Microbial suspensions of $1.5x10^8$ CFU/mL corresponding to 0.5 McFarland density obtained from 15-18 h bacterial cultures developed on solid media were used in our experiments. The tested substances were solubilised in DMSO and the starting stock solution was of 5000 µg/mL concentration. The qualitative screening was performed by an adapted disk diffusion method [49-53].

## 3. Results and discussions

### *3.1. IR Absorbance Spectra*

The FTIR spectra of Eu:HAp were recorded in the typical, absorption mode from KBr pellets.IR absorbance spectra of EuHAp samples with various europium concentrations ($0 \leq x_{Eu} \leq 0.2$) are shown in the 4000 $cm^{-1}$ to 400 $cm^{-1}$ range in Figure 1. Inourpreviousstudies [45] we haveshown that for all the samples the presence of strong $[OH]^-$ vibration peak (632 $cm^{-1}$) could be noticed. The broad bands in the regions 1600–1700 $cm^{-1}$ and 3200–3600 $cm^{-1}$ correspond to H–O– H bands of lattice water. Fowler B.O. in his infrared studies on apatites [54] showed that the band at 3570 $cm^{-1}$ is characterized by $[OH]^-$ stretching mode and the band at 632 $cm^{-1}$ characterized by $[OH]^-$ arises from stretching librational mode. The bands at around 1090 $cm^{-1}$ and about1040 $cm^{-1}$ can be attributed to the $\nu_3 [PO_4]^{3-}$ while the band at 962 arises from $\nu_1 [PO_4]^{3-}$. The 602 $cm^{-1}$ and 564 $cm^{-1}$ bands appear from $\nu_4 [PO_4]^{3-}$. Markovik et al. [55], presented that the sharpness of bands, especially sharpness of the 632

$cm^{-1}$, 602 $cm^{-1}$ and 564 $cm^{-1}$ bands indicate a well-crystallized HAp. The band at 475 $cm^{-1}$ can be attributed to the $\nu_2$ $[PO_4]^{3-}$ [56]. In the FT-IR spectrum of Eu:HAp with $x_{Eu} \geq 0.1$ (Figure 1) the bands corresponding to the $\nu_3$ vibration of C–O were observed at 1410 $cm^{-1}$, characteristic of the carbonate group [57-58].

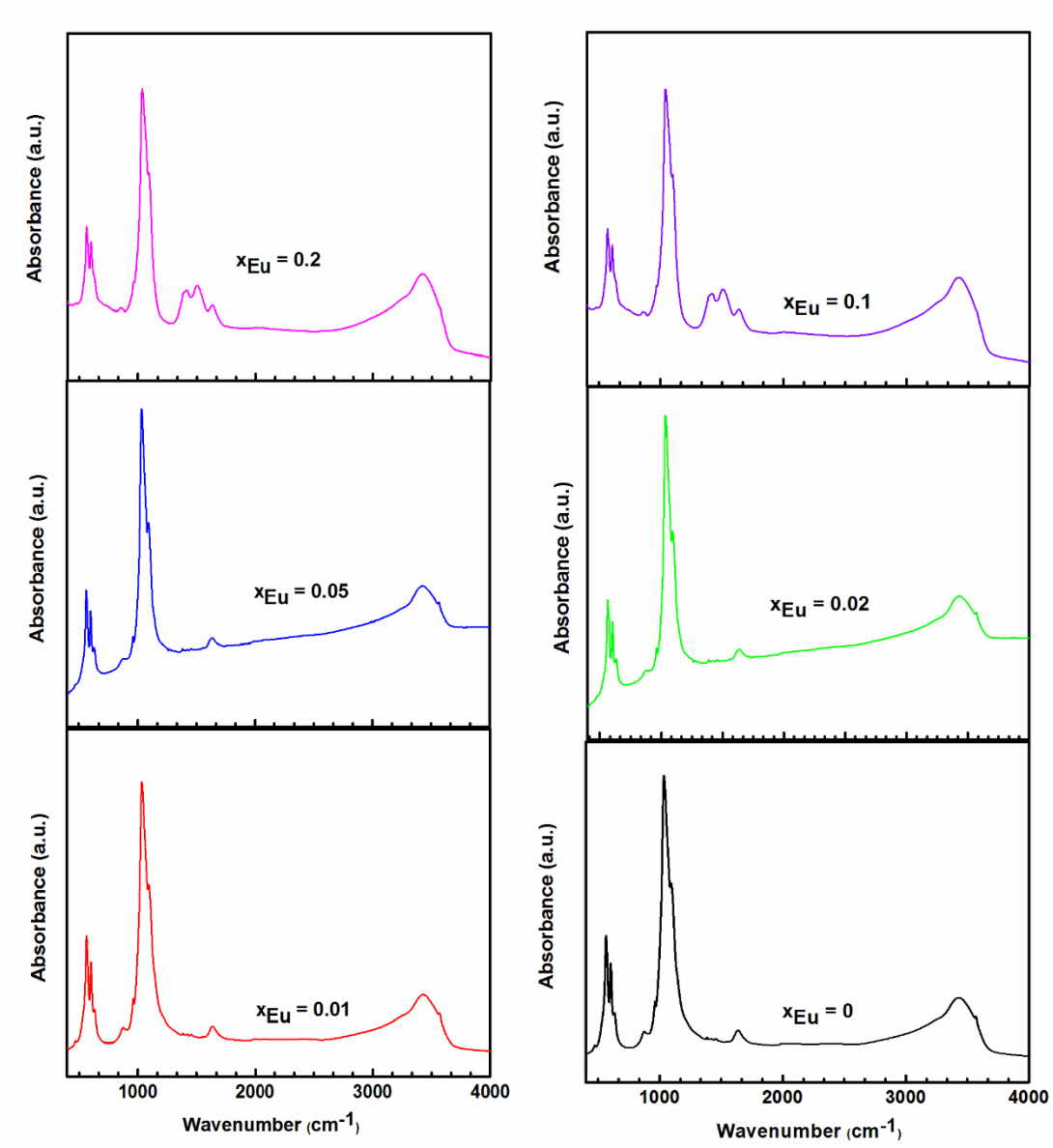


Figure 1: FT-IR spectra of europium doped hydroxyapatite (Eu:HAp) with $x_{Eu} = 0$, $x_{Eu} = 0.02$, $x_{Eu} = 0.2$.

The intensity of the band located at 1410 $cm^{-1}$ in the spectrum of Eu:HAp samples with $x_{Eu} \geq 0.1$ is attributed to components of the $\nu_3$ mode of a trace amount of $[CO_3]^{2-}$. The $\nu_2$ vibrations between 850 and 890 $cm^{-1}$, characteristic of the carbonate group were not

detected because $\nu_2$ $[CO_3]^{2-}$ band at 872 $cm^{-1}$ is hidden by $[HPO4]^{2-}$ band at 875 $cm^{-1}$. Similar comportment was observed by Markovik et al. [55] in his studies on preparation and comprehensive characterization of calcium hydroxyapatite. Markovik et al. and Holcomb D.W. et al. [59] showed that the $[CO_3]^{2-}$ band at 1410 $cm^{-1}$ derives from $[CO_3]^{2-}$ (designated by "B-type" carbonate that replace $PO_4^{3-}$ ions in the hydroxyapatite lattice). The band at 1510 $cm^{-1}$was also detected in the FT-IR spectrum of Eu:HAp with $x_{Eu} \geq 0.1$. The band at 1510 $cm^{-1}$ derives from $[CO_3]^{2-}$ (designated by "A-type" carbonate) that replaces$OH^-$ ions in the hydroxyapatite lattice [55, 60]. In all the spectra of Eu:HAp samples, the band at 875 $cm^{-1}$ was detected. This band is supposed to arise due to $[HPO_4]^{2-}$ ions from several reasons [55].

In Figure 1 we observed that the contribution of the area that corresponds to the phosphate bands decreases when the europium concentration in the samples increases. The bands at 475 and 962 $cm^{-1}$ progressively disappear with the increase of europium concentration. When the $x_{Eu} = 0.2$ the bands at 475 and 962 $cm^{-1}$ are almost absent. We can also observe in the Eu:HAp spectra a broadening of peak vibration with the decrease of the europium concentration. This behaviour was observed by Owada et al. [61] in sintered Y-doped hydroxyapatite.

### *3.2. IR Second Derivative Spectra*

In order to complete structural information on the analyzed Eu:HAp samples with $0 \leq x_{Eu} \leq 0.2$ we agreed to perform derivative analysis and peak fitting of selected $\nu_4$, $\nu_3$, $\nu_2$ and $\nu_1$phosphate bands. The second derivative of the spectrum of Eu:HAp samples ($x_{Eu} = 0$, $x_{Eu} = 0.02$, $x_{Eu} = 0.2$) in the $\nu_4$, $\nu_3$ and $\nu_1$ $[PO_4]^{3-}$ bands are shown in Figure 2.Only the results obtained for pure HAp ($x_{Eu} = 0$) and Eu:HAp ($x_{Eu} = 0.02$, $x_{Eu} = 0.2$) samples are shown, which clearly assigned the strong changes that occur in the FT-IR spectra of HAp in the presence of Eu. $\nu_1$ $[PO_4]^{3-}$ band was observed at around 962 $cm^{-1}$ in the second derivative spectra. On the other hand, in the second derivative spectra was identified a $\nu_2$ $[PO_4]^{3-}$ band at 475 $cm^{-1}$. In concordance with precedent studies, the bands assigned in the second derivative spectra of Eu:HAp ($0 \leq x_{Eu} \leq 0.2$) can beattributed to molecular vibrations of the phosphate $[PO_4]^{3-}$ in a apatitic stoichiometric environment of hydroxyapatite [62].

To evaluate the subtle spectral changes occurring as a consequence of the europium doped hydroxyapatite, the spectra in the spectral regions of 450–700 $cm^{-1}$($\nu_2$and $\nu_4$ $[PO_4]^{3-}$

domain) and 900–1200 $cm^{-1}$($\nu_1$ and $\nu_3$ $[PO_4]^{3-}$ domains) were analyzed by means of second derivative (Figure 2) and curve fitting analysis (Figure 3).

In Figure 2 we also observethe second derivative band at 633 $cm^{-1}$ that derives from the $OH^-$ librational mode. IR wavenumber position ($cm^{-1}$) of the $\nu_4$, $\nu_3$, $\nu_2$and $\nu_1$ $[PO_4]^{3-}$ bands of Eu:HAp spectrum from second derivative is presented in Table 1. Ten bands were detected for phosphate bands of hexagonal Eu:HAp samples.

Table 1. IR wavenumber position ($cm^{-1}$) of $\nu_4$, $\nu_3$, $\nu_2$ and $\nu_1$ $[PO_4]^{3-}$ bands of Eu:HAp spectrum from second derivative.

| Assignments | Position ($cm^{-1}$) | References |
|---|---|---|
| $\nu_1$ $[PO_4]^{3-}$ | 962 | 62 |
| $\nu_2$ $[PO_4]^{3-}$ | 475 | 62 |
| $\nu_3$ $[PO_4]^{3-}$ | 1033; 1045; 1073; 1090 | 62 |
| $\nu_4$ $[PO_4]^{3-}$ | 569; 575; 588; 602 | 62 |
| Present in newly precipitated apatite. | 1111 | 62-63 |
| $[HPO4]^{2-}$- containing apatites | 1144 | 63 |
| $[OH]^-$ group ( librational mode) | 633 | 63-64 |

Figure 3 shows the FT-IR spectrum of hydroxyapatite ($x_{Eu}$ = 0), the phosphate $\nu_4$, $\nu_3$, $\nu_2$ and $\nu_1$ regionswith experimental and calculated contours overlaid along with the individual subbands (blue) as determined by a curve fitting analysis. Five components were needed for a satisfactory fit in the spectral region of 450–700 $cm^{-1}$ ($\nu_2$ and $\nu_4$ $[PO_4]^{3-}$ domain) and eight in the spectral region of 900–1200 $cm^{-1}$($\nu_1$ and $\nu_3$ $[PO_4]^{3-}$ domains). FT-IR spectrum of Eu:Hap with $x_{Eu}$ = 0.02 is also presented and five components were needed for a satisfactory fit in the spectral region of 450–700 $cm^{-1}$($\nu_2$ and $\nu_4$ $[PO_4]^{3-}$ domain) and six in the spectral region of 900 –1200 $cm^{-1}$($\nu_1$ and $\nu_3$ $[PO_4]^{3-}$ domains). For Eu:Hap samples with$x_{Eu}$ =0.2 four components were needed for a satisfactory fit in the spectral region of 450–700 $cm^{-1}$ ($\nu_2$ and $\nu_4$ $[PO_4]^{3-}$ domain) and five important components in the spectral region of 900–1200 $cm^{-1}$ ($\nu_1$ and $\nu_3$ $[PO_4]^{3-}$ domains).

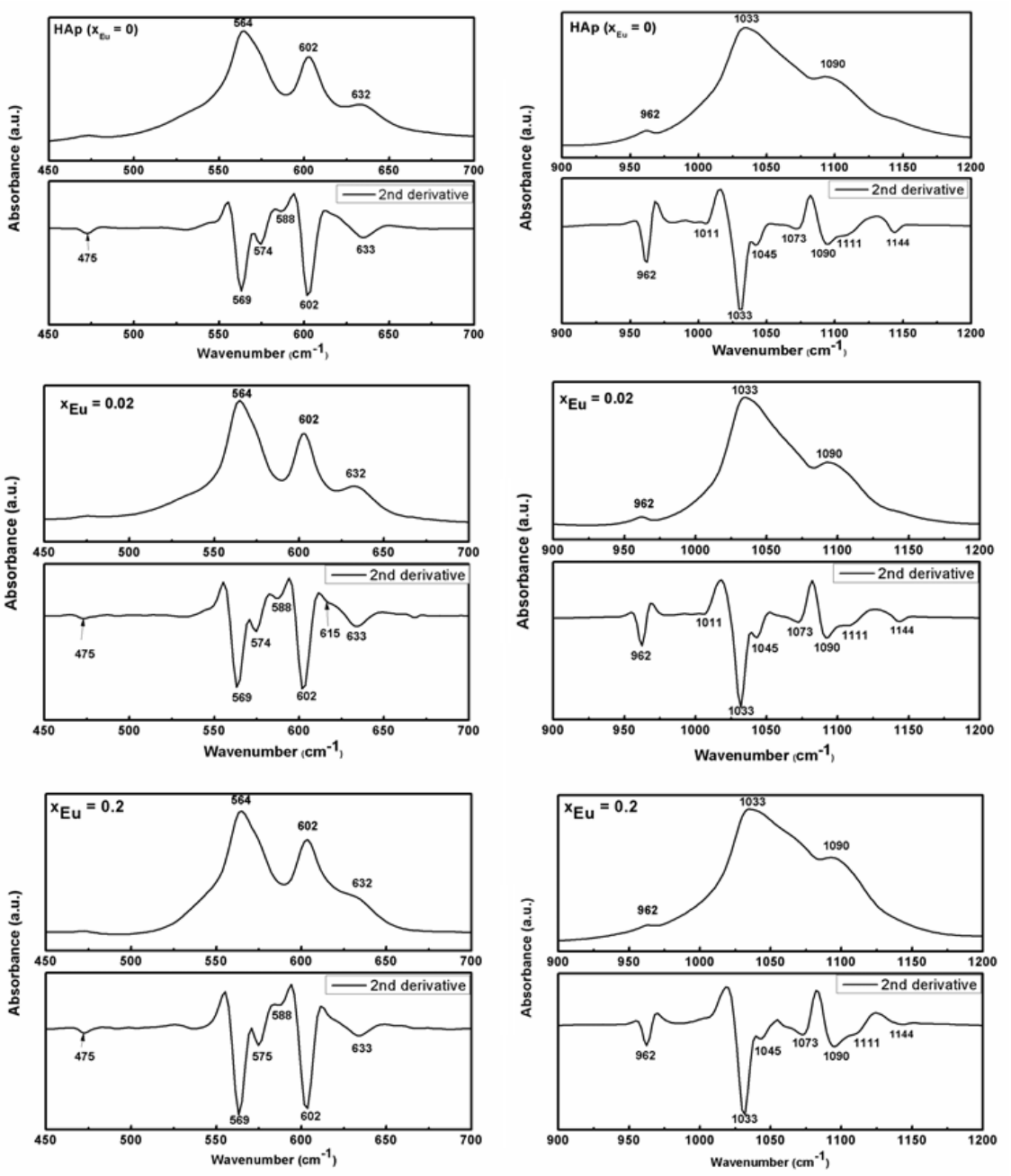


Figure 2: Second derivative of Eu:HAp ($x_{Eu}$ = 0, $x_{Eu}$ = 0.02, $x_{Eu}$ = 0.2) spectrum of the $\nu_4$, $\nu_3$, $\nu_2$ and $\nu_1$domains.

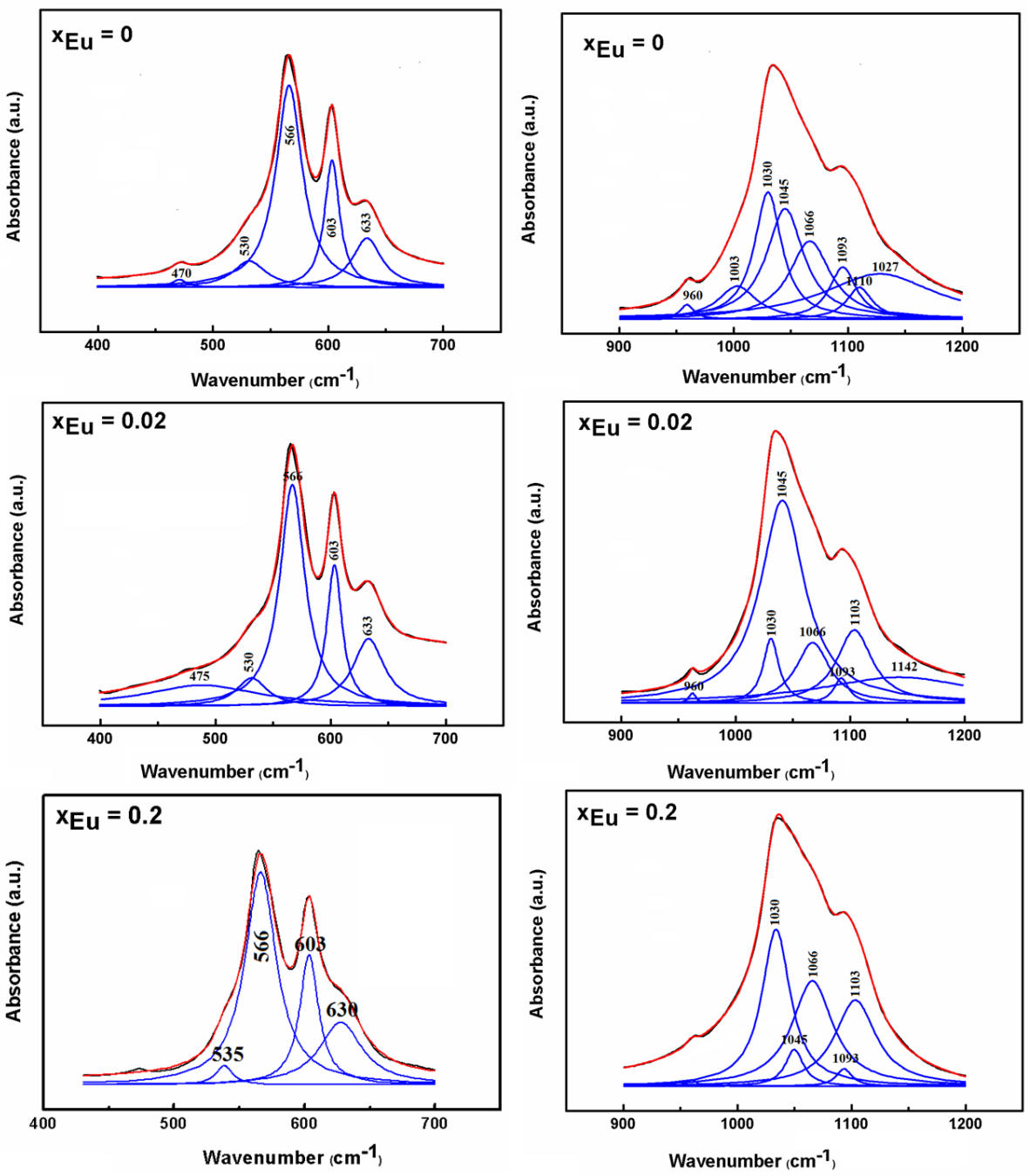


Figure 3: FT-IR deconvoluted spectra of the $\nu_4$, $\nu_3$, $\nu_2$ and $\nu_1$ domain for Eu:HAp ($x_{Eu}$ = 0, $x_{Eu}$ = 0.02, $x_{Eu}$ = 0.2).

The individual component for phosphate $\nu_2$ region (featured near 475 $cm^{-1}$) decreases for the samples with $x_{Eu}$ = 0.02 and disappears when $x_{Eu}$ increases to 0.2. The high frequency shoulder is more clearly defined for pure HAp than in the case of the Eu:HAp with $x_{Eu}$ = 0.02

and $x_{Eu}$ = 0.2 in the $\nu_1$ and $\nu_3$ phosphate regions. The band requires at least eight components for an adequate fit to the spectrum, compared with only six in the case of Eu:HAp with $x_{Eu}$ = 0.02 or only five in the Eu:HAp with $x_{Eu}$ = 0.2. In this series of materials it was not realistic to attempt to identify particular components characteristic the particle size. However, a correlation was found between the percentage area of the $\nu_1$, band (near 960 $cm^{-1}$) and the crystal size. The individual component for the phosphate $\nu_1$ region (band near 960 $cm^{-1}$) disappears when $x_{Eu}$ increases to 0.2. On the other hand, the individual component for phosphate $\nu_3$ region (band near 1040 $cm^{-1}$) decreases for the samples with $x_{Eu}$ = 0.02. However, in the Figure 2 and 3, we observe the disappearance of the band at 1144 cm-1, which is associated with $[HPO_4]^{2-}$ ions [65].We note that the main molecular species that gave rise to the Eu:Hap ($x_{Eu}$ = 0, $x_{Eu}$ = 0.02, $x_{Eu}$ = 0.2) absorbance in the 900-1200 $cm^{-1}$ region was assigned to the phosphate ion, $[PO_4]^{3-}$.

### *3.3. Antimicrobial studies*

A study on enhancement of osteoblast proliferation on europium doped hydroxyapatite has rarely been reported. Anselme K. [66] in his study concerning osteoblast adhesion on biomaterials and Garcia AJ, et al. [67] in the study of bio-adhesive surfaces to promote osteoblast differentiation and bone formation showed that often synthetic materials do not support osteoblast adhesion and this may result in poor cell differentiation and limited bone formation. Keselowsky BG et al. [68] in the study on surface chemistry and Mc Farland CD et al.[69] in his study on protein adsorption and cell attachment to patterned surfaces demonstrated that the effect of surface properties on cellular response depends on differences in species, concentration, and biological activity of adsorbed proteins, which may be obtained from different sources, i.e., biological fluids and cell-mediated synthesis and deposition.

The antimicrobial activity of Eu:HAp ($0 \leq x_{Eu} \leq 0.2$) nanoparticles was tested using the most common bacterial pathogens and fungus: *E coli ATCC 25922* (Gram-negative), *Pseudomonas aeruginosa 1397* (Gram-negative), *Staphylococcus aureus 0364* (Gram-positive), *Enterococcus faecalis ATCC 29212* (Gram-positive) and *Candida albicans ATCC 10231* (fungus).

The antimicrobial studies on Eu:HAp ($0 \leq x_{Eu} \leq 0.02$) nanoparticles indicated that antimicrobial activity is present.The results of antimicrobial activity of Eu:HAp ($0.05 \leq x_{Eu} \leq 0.2$) nanoparticles are shown in Figures 4-6. For the as-prepared Eu:HAp samples an

antibacterial activity was not observed on *E coli ATCC 25922* (Figures 4-6). The Eu:HAp nanoparticles with $x_{Eu}$ = 0.05 showed a good antibacterial activity on *Enterococcus faecalis ATCC 29212*) (Figure 6) for all the concentrations studied (from 0.031 mg/ml to 1 mg/ml). For the samples of Eu:HAp with $x_{Eu}$ = 0.1 and $x_{Eu}$ = 0.2 (Figures 5-6) we have observed that the inhibition of *Enterococcus faecalis ATCC 29212*) was more evident. In the samples with $x_{Eu}$ = 0.1, the inhibition was observed for concentrations higher than 0.062 mg/ml. For the as-prepared Eu:Hap samples with $x_{Eu}$ = 0.2 the inhibition was observed for all concentrations. For *Candida albicans ATCC 10231* a good inhibition was observed for samples with $x_{Eu}$ = 0.2 (Figure 6).

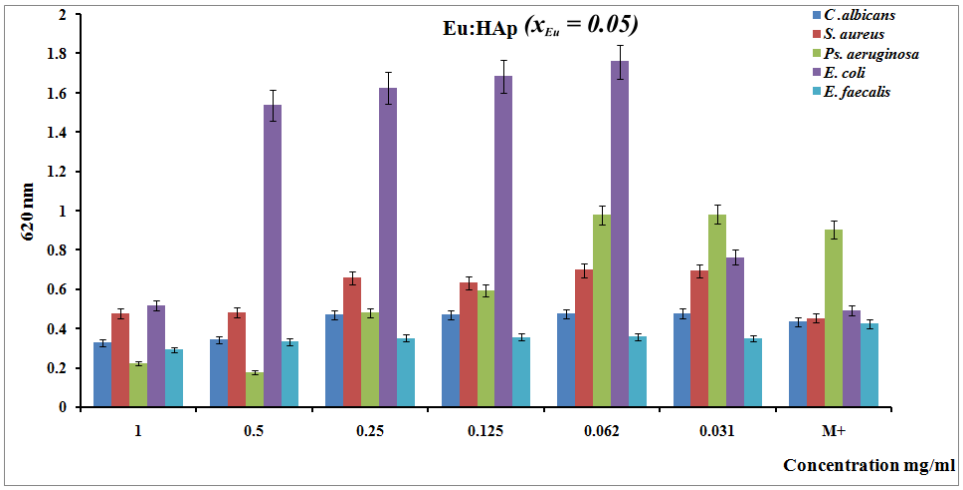


Figure 4:Antimicrobial activity of as-prepared Eu:HAp samples ($x_{Eu}$ = 0.05) on *E coli ATCC 25922*, *Pseudomonas aeruginosa 1397*, *Staphylococcus aureus 0364*, *Enterococcus faecalisATCC 29212* and *Candida albicans ATCC 10231*.

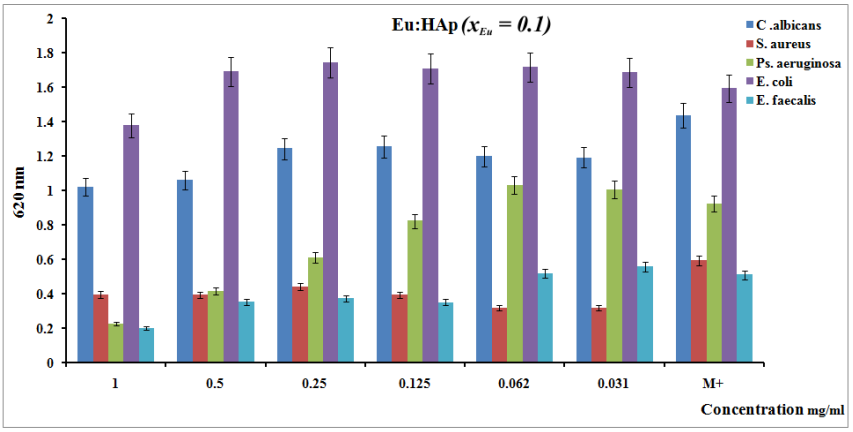

Figure 5: Antimicrobial activity of as-prepared Eu:HAp samples ($x_{Eu}$ = 0.1) on *E coli ATCC 25922, Pseudomonas aeruginosa 1397, Staphylococcus aureus 0364, Enterococcus faecalis ATCC 29212 and Candida albicans ATCC 10231*.

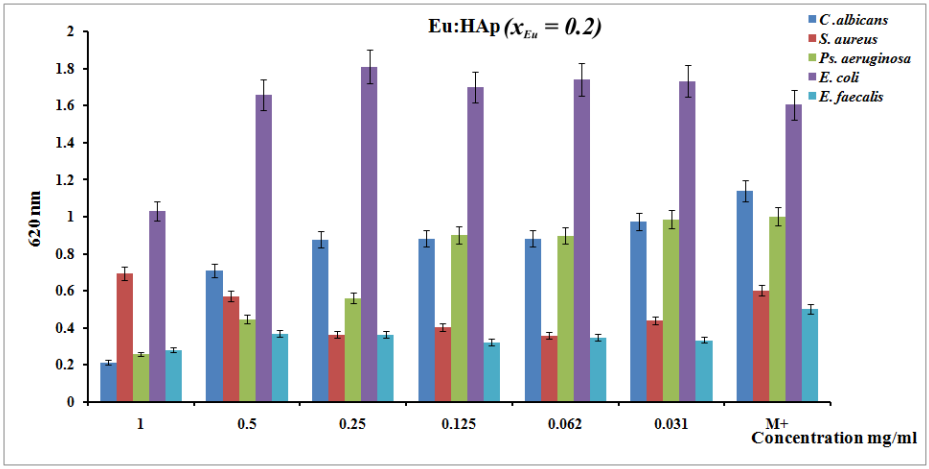


Figure 6: Antimicrobial activity of as-prepared Eu:HAp samples ($x_{Eu}$ = 0.2) on *E coli ATCC 25922, Pseudomonas aeruginosa 1397, Staphylococcus aureus 0364, Enterococcus faecalis ATCC 29212 and Candida albicans ATCC 10231*.

For samples with $x_{Eu}$ = 0.05 and $x_{Eu}$ = 0.1 the inhibition was observed at high concentrations (Figures 4-6). Additionally, a very good inhibition of *Pseudomonas aeruginos*a 1397 has been noticed when the concentration of Eu:Hap ($0.05 \leq x_{Eu} \leq 0.2$) increased from 0.125 mg/ml to 1 mg/ml. Raimondi et al. [70] and Morones et al.[71], studying the inhibition of bacterial growth by differentially shaped nanoparticles, showed that the antimicrobial efficacy of the nanoparticles depends on the shape of the nanoparticles.

One of the aims of this study was to obtain an Eu:Hap stoichiometric apatite and to contribute to the study of the influence of europium in the structure of hydroxyapatite. We note that it is possible to determine the type of apatite, nonstoichiometric or stoichiometric, using Fourier deconvolution techniques. This study allowed highlighting the stoichiometry of Eu:HAp biomaterials, based on changes in the phosphate $\nu_1$ and $\nu_3$ absorbances in the 900-1200 $cm^{-1}$ spectral region. The Sauer GR et al. [72] in their studies claimed that the presence of the $[PO_4]^{3-}$ doublet at 602 and 567 $cm^{-1}$ in all the composites suggest that the precursor phase of the HAp was octacalcium phosphate, OCP, ($Ca_8H_2[PO_4]_6$). On the other hand, they

showed that the OCP precursor ensures a more crystalline and ordered HAp phase. Granja PL et al. [73] in their previous studies have affirmed that if the precursor had been amorphous calcium phosphate (ACP) ($Ca_2[PO_4]_3$), these $[PO_4]^{3-}$ bands should be a broad singlet instead of a doublet. Moreover, Hutchens SA et al. in 2006 [74] evidenced that ACP precipitation requires the rapid interaction between $Ca^{2+}$ and $[PO_4]^{3-}$at high supersaturation instead of precursor complexation with other species. A previous study of apatite minerals realized by Rey et al. in 1991 [75], using Fourier deconvolution analysis, has attributed a 1020 $cm^{-1}$ band to nonstoichiometric apatite containing $[HPO_4]^{2-}$ and $[CO_3]^{2-}$, and the band at 1125$cm^{-1}$in FT-IR deconvoluted spectra to stoichiometric apatite. Due to the presence of the band at around 1127 $cm^{-1}$ in all the prepared samples, our present studies have shown that the Eu:HAp is a stoichiometric apatite.

Moreover, our present study demonstrates that the antibacterial activity of Eu:HAp nanoparticles is dependent on the europium concentration. Furthermore, the inhibitory effect was found to be dependent to the increase of concentration from 0.031 mg/ml to 1 mg/ml.

## Conclusions

In the present work, we contributed to the study of the influence of europium in structure of hydroxyapatite. Using Fourier deconvolution techniques we showed that it is possible to determine the type of Eu:HAp apatite, nonstoichiometric or stoichiometric. The spectra of Eu:Hap samples in the spectral regions of 450–700 $cm^{-1}$ and 900–1200 $cm^{-1}$ were analyzed by means of second derivative and using Fourier deconvolution analysis. This study allowed highlighting the stoichiometry of Eu:HAp biomaterials, based on changes in the phosphate $\nu_1$ and $\nu_3$ absorbances in the 900-1200 $cm^{-1}$ spectral region.

The antimicrobial activity of Eu:HAp ($0 \leq x_{Eu} \leq 0.2$) nanoparticles was tested using the most common bacterial pathogens and fungus: *E coli ATCC 25922* (Gram-negative), *Pseudomonas aeruginosa* (Gram-negative), *Staphylococcus aureus 0364* (Gram-positive), *Enterococcus faecalis ATCC 29212* (Gram-positive) and *Candida albicans ATCC 10231*(fungus).

In summary, this study on the antimicrobial activity of Eu:HAp ($0 \leq x_{Eu} \leq 0.2$) nanoparticlesdescribes a nanotechnology-based strategy luminescent $Eu^{3+}$ doped hydroxyapatite represents a potential application for drug release and targeting based on their luminescent properties. These results and methods could be interesting for academic and

industrial researchers in biomaterials, potential orthopedic medical materials and drug carriers.

**Competing interests**

The authors declare that they have no competing interests.

**Acknowledgments**

The financial and encouragement support provided by the Ministery of Educations of Romaniaunder the project IFA-CEANo. C2-06. The authors gratefully acknowledgments the support given to this work by Dr. F. Massuyeau from Institut des Matériaux-Jean Rouxel, Nantes.

**References**

1. LeGerosR Z, LeGeros JP:Calcium phospate bioceramics:past, present, future. *Key Eng Mater* 2003, 3:240–242.

2. Hench LL,Wilson J: Suface Active Biomaterials. *Science*1984, 226:630-636.

3. Suchanek W, Yoshimura M: Processing and properties of hydroxyapatite based biomaterials for use as hard tissue replacement implants. *J Mater Res* 1998,13:94-117.

4.Srinivasa Rao Ch, Upendra Kumar K, Jayasankar C K: Luminescence properties of $Eu^{3+}$ ions in phosphate-based bioactive glasses. *Solid State Sci* 2011,13(6):1309-1314.

5. Hench LL, Splinter RJ, Allen WC, Greenlee TK: Bonding mechanism at the interface of ceramic prosthetic materails. *J Biomed Mater Res* 1971, 2:117-141.

6.Izquierdo-Barba I, Vallet Regi M: Fascinating properties of bioactive templated glasses: A new generation of nanostructured bioceramics.*Solid State Sci*2011,13:773-783.

7.Vallet-Regí M, Balas F, Arcos D: Mesoporous materials for drug delivery. *Angew Chem Int Ed* 2007,46:7548–58.

8.Hench LL, Polak JM: Third Generation Biomaterials. *Science* 2002, 295(5557):1014-1017.

9.Arcos D, Del Real RP, Vallet-Regí M: Biphasic materials for bone grafting and hyperthermia treatment of cancer. *J Biomed Mater Res A* 2003,65:71–78.

10.Hench LL: Bioceramics: from concept to clinic. *J Am Ceram Soc*1991,74:1487–510,.

11. Rao JH, Dragulescu-Andrasi A, YaoH Q: Fluorescence imaging in vivo: recent advances.*Curr Opin Biotechnol* 2007,18:17-25.

12. Zhou J, Sun Y, Du XX, Xiong LQ, Hu H, Li FY: Dual-modality in vivo imaging using rare-earth nanocrystals with near-infrared to near-infrared (nir-to-nir) upconversion luminescence and magnetic resonance properties. *Biomaterials* 2010, 31:3287-95.

13. Chen F, Huang P, Zhu Y-J, Wu J, Cui D-X: Multifunctional $Eu^{3+}$/$Gd^{3+}$ dual-doped calcium phosphate vesicle-like nanospheres for sustained drug release and imaging. *Biomaterials* 2012, 33:6447-6455.

14. Dembski S, Rupp S, Milde M, Gellermann C, Dyrba M, Schweizer S, Batentschuk M, Osvet A,Winnacker A: Synthesis and optical properties of luminescent core–shell structured silicate and phosphate nanoparticles. *Opt Mater* 2011, 33(7):1106-1110.

15. Chander H: Development of nanophosphors - A review. *Mater Sci Eng R* 2005,49(5):113–155.

16.Höppe HA: Recent developments in the field of inorganic phosphors. *Angew Chem Int Ed* 2009,48(20):3572–3582.

17. Shen J, Sun L-D, Yan C-H: Luminescent rare earth nanomaterials for bioprobe applications. *Dalton Transactions* 2008,42:5687–5697.

18. De Araujo TS, Macedo ZS, De Oliveira P, Valerio M: Production and characterization of pure and $Cr^{3+}$-doped hydroxyapatite for biomedical applications as fluorescent probes. J *MaterSci* 2007,42:2236–43.

19.Jagannathan R, Kottaisamy M: $Eu^{3+}$ luminescence: A spectral probe in $M_5(PO_4)_3X$ apatites (M=Ca or Sr; X=$F^-$, $Cl^-$, $Br^-$ or $OH^-$). *J Phys Condens Matter*, 1995,7 (44):8453.

20. Graeve OA, Kanakala R, Madadi A, Williams BC, Glass KC: Luminescence variations in hydroxyapatites doped with $Eu^{2+}$ and $Eu^{3+}$ ions. *Biomaterials* 2010,31:4259–4267.

21. Dittmeyer R, Keim RW, Reysa G, Oberholz A. in Chemische Technik: Prozesse und Produkte. Band 2: Neue Technologie. Wiley-VCH, Weinheim 2004.

22.Tissue BM: Synthesis and luminescence of lanthanide ions in nanoscale insulating hosts. *Chem Mater* 1998,10:2837-2845.

23. Groza A: Review of the processes identified during the polymerization of organic and organosilicon liquid films in atmospheric pressure air corona discharges. *Rom Rep Phys* 64, 2012:1227–1242.

24.Wang F, Tan WB, Zhang Y, Fan X, Wang M: Luminescent nanomaterials for biological labelling. *Nanotechnology* 2006,17(1): R1–R13.

25. Meiser F, Cortez C, Caruso F: Biofunctionalization of Fluorescent Rare-Earth-Doped Lanthanum Phosphate Colloidal Nanoparticles. *Angew Chem Int Ed* 2004,43:5954-5957.

26. Han Y, Wang X, Dai H, Li S: Synthesis and luminescence of $Eu^{3+}$ doped hydroxyapatite nanocrystallines: Effects of calcinations and $Eu^{3+}$ content. *J Lumin* 2012, 135:281-287.

27. Rakovan J, Reeder RJ: Intracrystalline Rare Earth Element distributions in apatite: Surface structural influences on zoning during Growth. *Geochim Cosmochim Acta* 1996, 60:4435-4445.

28.Reisfeld R, Gaft M, Boulon G, Panczer G, Jorgensen CK: Laser-induced luminescence of rare-earth elements in natural fluor-apatites. *J Lumin* 1996, 69:343-353.

29.Mayer I, Layani JD, Givan A, Gaft M, Blanc P: La ions in precipitated hydroxyapatites. *J Inorg Biochem* 1999,73(4):221-226.

30. Martin P, Carlot G, Chevarier A, Den-Auwer C, Panczer G: Mechanisms involved in thermal diffusion of rare earth elements in apatite. *J Nucl Mater* 1999, 275:268-276.

31. Doat A, Fanjul M, Pelle F, Hollande E, Lebugle A: Europium-doped bioapatite: a new photostable biological probe, internalizable by human cells. *Biomaterials* 2003,24:3365-3371.

32. Doat A, Pelle F, Gardant N, Lebugle A: Synthesis of luminescent bioapatite nanoparticles for utilization as a biological probe. *J Solid State Chem* 2004, 177:1179-1187.

33.Doat A, Pellé F, Lebugle A: Europium-doped calcium pyrophosphates : allotropic forms and photoluminescent properties. *J Solid State Chem* 2005, 1(7):2354-2362.

34.Mondejar SP, Kovtun A, Epple M: Lanthanide-doped calcium phosphate nanoparticles with high internal crystallinity and with a shell of DNA as fluorescent probes in cell experiments. *J Mater Chem* 2007,17:4153–4159.

35.Ciobanu CS, Iconaru SL, Le Coustumer P, et al.: Antibacterial activity of silver-doped hydroxyapatite nanoparticles against gram-positive and gram-negative bacteria. *Nanoscale Res Lett* 2012,7:324.

36. Ciobanu CS, Massuyeau F, Andronescu E, Stan MS, Dinischiotu A, Predoi D: Biocompatibility Study Of Europium Doped Crystalline Hydroxyapatite Bioceramics. *Dig J Nanomater Bios* 2011,6(4):1639-1647.

37. Capobianco JA, Proulx PP, Raspa N: Laser-excited fluorescence spectroscopy and crystal field analysis of europium (III)-doped cordierite glass. *Chem Phys Lett* 1989,160:591-596.

38.Lavin V, Babu P, Jayasankar CK, Martin IR, Rodriguez VD: On the local structure of $Eu^{3+}$ ions in oxifluoride glasses. Comparison with fluoride and oxide glasses. *J Chem Phys* 2001, 115(23):10935-10944.

39. Zambelli M, Abril M, Lavin V, Speghini A, Bettinelli M: Fluorescence line narrowing spectroscopy of $Eu^{3+}$ in a niobium tellurite glass. *Phys Non-Crystalline Solids* 2004, 345–346(15):386–390.

40. KushidaT: Site-selective fluorescence spectroscopy of $Eu^{3+}$ and $Sm^{2+}$ ions in glass. *J Lumin* 2002,100(1–4):73-88.

41. Doweidar H: Density–structure correlations in Na2O–CaO–P2O5–SiO2 bioactive glasses. *J Non-Cryst Solids* 2009, 355(9):577-580.

42. Frost RL, Mills SJ, Weier ML: Peisleyite an unusual mixed anion mineral—a vibrational spectroscopic study. *Spectrochim Acta Part A* 2005,61(1–2):177-184.

43. Fleet ME, Liu X: Coupled substitution of type A and B carbonate in sodium-bearing apatite. *Biomaterials* 2007, 28(6):916-926.

44. Sivakumar M, Sampath Kumart TS, Shantha KL, Panduranga Rao K: Development of hydroxyapatite derived from Indian coral. *Biomaterials* 1996,17(17):1709-1714.

45.Ciobanu CS, Iconaru SL, Massuyeau F, Constantin LV, Costescu A, Predoi D: Synthesis, Structure, and Luminescent Properties of Europium-Doped Hydroxyapatite Nanocrystalline Powders. *J Nanomater* 2012, doi:10.1155/2012/942801.

46. Kolmas J, Jaklewicz A, Zima A, Bućko M, Paszkiewicz Z, Lis J, Ślosarczyk A, Kolodziejski W: Incorporation of carbonate and magnesium ions into synthetic hydroxyapatite: The effect on physicochemical properties. *J Mol Struct* 2011,987:40–50.

47. Matsuhiro B, Rivas P: Second-derivative Fourier transforms infrared spectra of seaweed galactans. *J Appl Phycol* 1993,5(1):45-51.

48. Gómez-Ordóñez E, Rupérez P: FTIR-ATR spectroscopy as a tool for polysaccharide identification in edible brown and red seaweeds. *Food Hydrocolloids* 2011,25:1514-1520.

49. Uggeri J, Guizzardi S, Scandroglio R, Gatti R: Adhesion of human osteoblasts to titanium: A morpho-functional analysis with confocal microscopy", *Micron* 2010,41:210–219.

50. Buttke TM, McCubrey JA, Owen TC: Use of an aqueous soluble tetrazolium/formazan assay to measure viability and proliferation of lymphokine-dependent cell lines. *J Immunol Methods*1993,157(1–2):233–240.

51. Limban C, Chifiriuc MC: Antibacterial Activity of New Dibenzoxepinone Oximes with Fluorine and Trifluoromethyl Group Substituents. *Int Journal Mol Sci* 2011,12(10):6432-6444.

52. Limban C, Marutescu L, Chifiriuc MC: Synthesis, Spectroscopic Properties and Antipathogenic Activity of New Thiourea. *Derivatives Molecules* 2011, 16(9):7593-7607.

53. Marutescu L, Limban C, Chifiriuc MC, Missir A-V, Chirita IC, Caproiu MT: Studies on the antimicrobial activity of new compounds containing thiourea function. *Biointerface Research in Applied Chemistry* 2011,1(6):236-241.

54. Fowler BO: Infrared studies on apatites. I. Vibrational assignment for calcium, strontium and barium hydroxyapatites utilizing isotopic Subtitutions. *Inorg Chem* 1974,13:194-207.

55.Markovik M, Fowler BO, Tung MS: Preparation and comprehensive characterization of a calcium hydroxyapatite reference material. *J Res Natl Inst Stan* 2004,109:553-568.

56. Jastrzebski W, Sitarz M, Rokita M, Bułat K: Infrared spectroscopy of different phosphates structures, *Spectrochimica Acta Part* A, 2011,79:722-727.

57. Nakamoto K In: Nakamoto K: Infrared and Raman spectra of inorganic and coordination compounds. *New York: Wiley* 1978.

58. LeGeros RZ, Bonel G, Legros R: Types of ‘‘$H_2O$’’ in human enamel and in precipitated apatites. *Calcif Tissue Res* 1978, 26:111–118.

59. Holcomb DW, Yung RA: Thermal decomposition of human tooth enamel, *Calcified Tissue International*1980,31:189-20.

60. Elliott JC: The crystallographic structure of dental enamel and related apatites. *PhD Thesis, University of London*1974.

61. Owada H, Yamashita K, Umegaki T, Kanazawa T, Nagai M: Humidity-sensitivity of yttrium substituted apatite ceramics. *Solid State Ionics* 1989,35(3-4):401–404.

62. Castro Ribeiro C, Gibson I, Barbosa MA: The uptake of titanium ions by hydroxyapatite particles-structural changes and possible mechanisms. *Biomaterials* 2006, 27:1749–1761.

63. Rey C, Shimizu M, Collins B, Glimcher MJ: Resolution enhanced Fourier transform infrared spectroscopy study of the environment of phosphate ion in the early deposits of a solid phase calcium phosphate in bone and enamel and their evolution with age: investigations in the n3 PO43domain. *Calcif Tissue Int* 1991,49:383–388.

64. Kay MI, Young RA, Posner AS: Crystal structure of hydroxyapatite. *Nature* 1964, 204:1050–2.

65. Paluszkiewicz C, Slosarczyk A, Pijocha D, Sitarz M, Bucko M ,Zima A, Chroscicka A, Lewandowska-Szumieł M: Synthesis, structural properties and thermal stability of Mndoped hydroxyapatite, *Journal of Molecular Structure*, 2010, 976:301-309.

66. Anselme K: Osteoblast adhesion on biomaterials. *Biomaterials* 2000, 21:667–81.

67. Garcia AJ, Reyes CD: Bio-adhesive surfaces to promote osteoblast differentiation and bone formation. *Journal of Dental Research* 2005, 84:407–13.

68. Keselowsky BG, Collard DM, Garcia AJ: Surface chemistry modulates focal adhesion composition and signaling through changes in integrin binding. *Biomaterials* 2004, 25:5947–54.

69. McFarland CD, Thomas CH, De Filippis C, Steele JC, Healy KE: Protein adsorption and cell attachment to patterned surfaces. J *Biomed Mater Res* 2000, 49:200–10.

70. Raimondi F, Scherer GG, Kotz R, Wokaun A: Nanoparticles in energy technology: examples from electochemistry and catalysis. *Angew Chem Int Ed* 2005,44:2190-2209.

71. Morones JR, Elechiguerra JL, Camacho A, Ramirez JT: The bactericidal effect of silver nanoparticles. *Nanotechnology* 2005,16:2346-2353.

72. Sauer GR, Wuthier R E: Fourier transform infrared characterization of mineral phases formed during induction of mineralization bycollagenase-released matrix vesicles in vitro. *The Journal of Biological Chemistry* 1988, 27:13718–24.

73. Granja PL, Barbosa MA: Cellulose phosphates as biomaterials. Mineralization of chemically modified regenerated cellulose hydrogels. *J Mater Sci*2001,36:2163–72.

74. Hutchens SA, Benson RS, Evans BR, O'NeillH M, Rawn CJ: Biomimetic synthesis of calcium-deficient hydroxyapatite in a natural hydrogel. *Biomaterials* 2006,27:4661–4670.

75. Rey C, Shimuzu M, Collins B, Glimcher MJ: Resolution enhanced fourier transform infrared spectroscopy study of the environment of phosphate ions in the early deposits of a solid phase of calcium-phosphate in bone and enamel, and their evolution with age. I. Investigations in the v4 P04 domain.*Calcif Tissue Int* 1990, 46:384-394.